

Invasiveness of pico- and nanosecond E-FISH on plasma bullets in nitrogen

A.A.A. Limburg¹, T.E.W. Keur¹, R.F.E. Pleijers¹ and S. Nijdam¹

¹Department of Applied Physics, Eindhoven University of Technology, PO box 513, 5600 MB Eindhoven, The Netherlands

E-mail: a.a.a.limburg@tue.nl

Abstract. The electric field is the driving force behind every plasma. Electric field induced second harmonic generation (E-FISH) is a diagnostic able to obtain the electric field with high temporal and spatial resolution, is considered non-invasive and can be applied to almost any type of plasma with high sensitivity. However, the high power laser beam used as a probe in this technique, can interact with the gas and induce charges, which can subsequently influence the plasma. In this work, E-FISH is applied on non-thermal pulsed plasma jets in N₂ flowing into atmospheric air. In these jets, ionization fronts propagate along the axis of the jet, which are highly reproducible and periodic. This allows for phase resolved measurements. A nanosecond and a picosecond pulsed laser, both operating at 1064 nm, are used as sources. For the first time, the obtained E-FISH signals measured with both lasers are compared to each other. The results deviate significantly between the two lasers, which can be explained by laser induced guiding of the streamers. This is observed by taking ICCD images of the plasma trajectory. At the position where the plasma crosses the laser beam path, the plasma branches. This reveals that E-FISH is also invasive under some conditions. The profiles obtained with the picosecond laser are in good qualitative agreement with previous coherent Raman scattering-based four-wave mixing results on the same plasma source and therefore the picosecond laser is considered non-invasive. In future E-FISH measurements, the influence of the laser beam on the E-FISH signal should be taken into account to prevent changing the plasma behavior. By decreasing the laser power or using a shorter laser pulse, successful measurements can be performed.

1. Introduction

Laser diagnostics allow for localized, unobstructed and direct detection of all kinds of plasma parameters. For example, Thomson scattering, which is the scattering of laser light on free electrons, is used to determine electron density and electron temperature [1]. The electric field is the driving force behind every plasma. It determines the production of energetic particles, energy losses, gas temperature and chemical activity [2]. Therefore, information on the spatial and temporal distribution of the

electric field could, for example, be used to enable gas temperature control throughout a plasma, which is essential in medical applications. A tool for measuring the electric field of discharges has been desired by the plasma community for decades. Several methods are used in previous studies. However, direct electric field measurements on transient discharges are often invasive or limited by photon emission and assumptions [3]. Electric field measurements based on the Stark effect are, for instance, based on emission spectroscopy. Therefore, the range over which the field can be determined is limited to the spatial and temporal range in which light is emitted by the plasma during a discharge [4, 5]. Another approach is to introduce a birefringent target surface [6, 7]. The electric field of the plasma, impinging on the target, changes the refractive index of the target material. By measuring this change, the electric field of the plasma can be determined. These measurements are highly relevant in the material science industry or plasma medicine, in which a target is used. However, the electric field of the discharge is influenced by the presence of the target [8].

In this work, an optical probe measurement technique to measure electric fields that overcomes these disadvantages, is tested and developed. This technique, called electric-field induced second harmonic generation (E-FISH), has just become available, is easy to implement and shows great promise for a wide variety of plasmas [9, 10]. A nanosecond pulsed and a picosecond pulsed Nd:YAG laser, both emitting at 1064 nm, are used as sources and non-linearly interact with an electric field. In this way, information on the spatial and temporal development of the field strength and polarization is obtained. The E-FISH technique is tested on plasma bullets in N₂ flowing into atmospheric pressure air. Plasma bullets are guided streamer discharges. The high reproducibility of guided streamer discharges in pulsed plasma jets, which allows for phase resolved measurements, is generally ascribed to a memory effect, where the seed electrons for the next discharge are provided by remnants of the previous discharges [11–13]. The bullets cross the beam path in the focus.

So far, laser diagnostics, including E-FISH, are generally considered non-invasive when applied to plasma [14]. This makes them advantageous over most other plasma diagnostics. However, laser beams can induce the guiding of streamer discharges, such as plasma bullets, due to photoionisation or photodetachment of the medium through which the bullets move [15, 16]. If this occurs, the electric field profile of the plasma can change during the E-FISH measurement due to the laser beam. As a consequence, these measurements can no longer be deemed accurate and the technique has to be considered invasive. This would make E-FISH unsuitable to gain understanding about the discharge itself. In a recent paper of Nakamura [17] on E-FISH, the occurrence of laser induced streamers is described, but these discharges do not affect the E-FISH signal.

In this work, the knowledge about the limitations and the possibilities of E-FISH as a new method to determine electric fields is extended by analyzing the impact of the laser beam on a plasma bullet. The effect of the pulse duration of this beam is investigated in regard to the accuracy of obtained electric field measurements, as well

as the invasiveness on the plasma.

In order for a non-linear interaction, such as second harmonic generation, to occur, a high intensity input beam is needed. Moreover, the E-FISH signal intensity scales as the square of the input intensity. Consequently, short, high energy laser pulses of the order of hundreds of picoseconds or less are preferred. Another advantage of shorter laser pulses is that the pulse energy, which is constrained by laser-induced breakdown [18], is lower, while the beam intensity is higher. Laser-induced breakdown can influence the measured second harmonics (SH), either by disturbing the to-be-measured electric field or by generating light in the wavelength range for which the detector is sensitive. Furthermore, the time resolution of the E-FISH measurements is limited to the pulse duration of the laser source. Thus, for transient discharges, of which the electric field can vary on sub-nanosecond timescales, a nanosecond pulse duration may prove limiting. The E-FISH technique has been applied to electric fields in air using nanosecond, picosecond and femtosecond lasers [9, 19, 20]. However, the intrusiveness of the laser beams as a function of the pulse duration on the plasma was not experimentally assessed.

This paper reveals that nanosecond E-FISH can be invasive when applied to plasma bullets and results need to be critically assessed. Furthermore, a picosecond laser beam can induce branching of the bullets. This will be a crucial extension to the fundamental knowledge of the E-FISH technique as it largely determines the accuracy of the results.

2. Experimental setup

In figure 1, a schematic of the used setup is presented. Two different Nd:YAG lasers are used in this study, both emitting at 1064 nm: a Quantel Q-smart 450, which emits 6 ns pulses at a frequency of 20 Hz and an Ekspla 312 which emits 150 ps pulses beam at a frequency of 10 Hz. A laser beam emitted by one of these sources interacts non-linearly with an electric field, which results in frequency doubled light (SH). The input polarization of the laser light is controlled to achieve maximum second harmonic generation, e.g. the input light polarization is parallel to the to-be-measured field direction. Subsequently, the laser beam is focused into the measurement area using a plano-convex lens of 500 mm focal length. Characteristics of the used plasma source can be found in [21]. To summarize: a pulsed plasma jet is generated by applying high voltage (HV) pulses to the plasma source using a HV power supply (Spellman SL50N150X4256), which is gated by a HV pulse generator (DEI PVX-4110), in pure N₂ (99.999%), injected via a feed gas inlet at a volumetric flow rate of 1 standard litre per minute (slm). The HV pulses are set to be 500 ns wide, with rise and fall times of about 40 ns. The discharges are produced at a repetition frequency of 3 kHz at a fixed voltage amplitude of 8 kV. For precise positioning of the plasma bullets inside the laser beam, a motorized translation stage is used (Zaber Technologies T-XYZ-LSM050A). The shape of the plasma is monitored by an ICCD camera (Andor iStar CCD DH334T-18U-E3) with a Nikon UV 105 mm f/4.5 lens, which is shown in figure 2. The gate of the camera is either set to 2 ns or 170 ns/220 ns, to capture the propagation of a

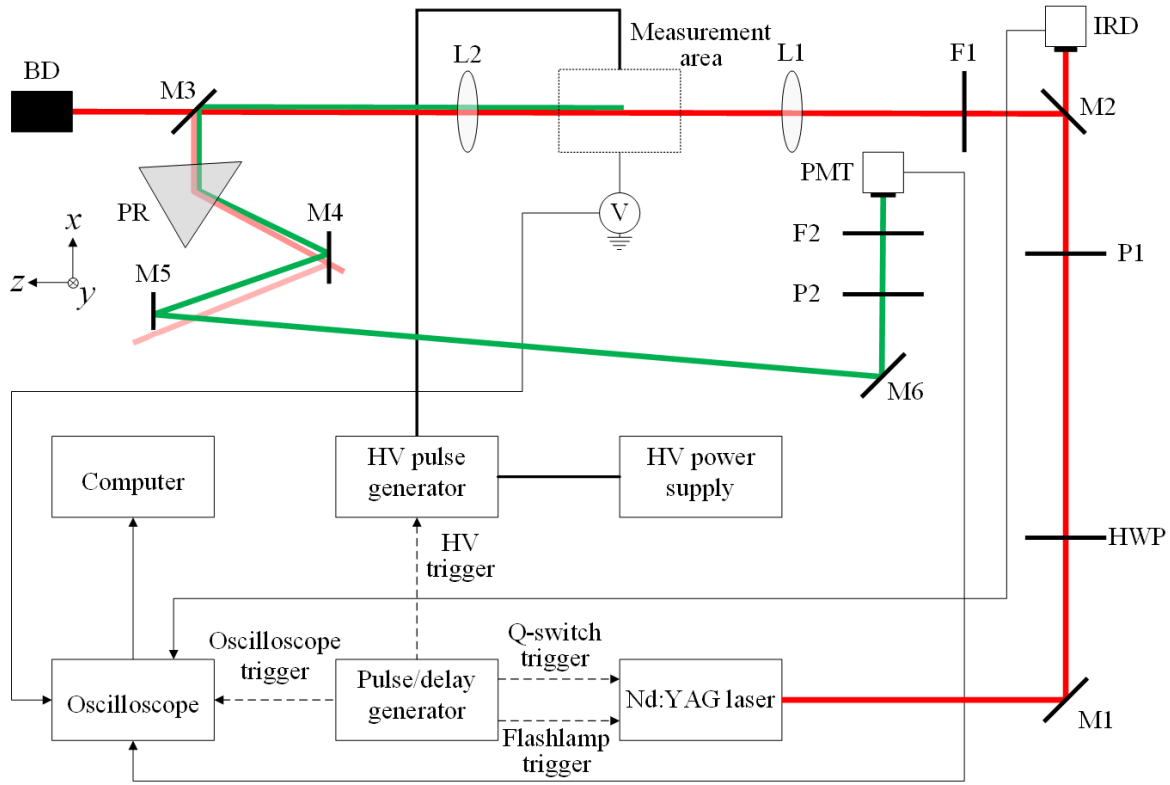


Figure 1: Schematic drawing of the experimental setup used for E-FISH measurements. The infrared laser beam is indicated in red, while the SH beam is indicated in green. M1: dielectric mirror; HWP: 1064 nm half-wave plate; P1: 1064 nm polarizer; M2: backside polished mirror; F1: 1064 nm bandpass filter; L1 & L2: plano-convex lenses; M3, M4, M5: dichroic mirrors (532 nm reflecting, 1064 nm transmitting); PR: prism; M6: dielectric mirror; P2: 532 nm polarizer; F2: 532 nm bandpass filter; BD: beam dump; IRD: infra-red detector; PMT: photomultiplier tube. The infra-red light is focused by L1 and collimated by L2. Furthermore, after the SH light is generated, both beams are colinear until they are separated by the prism.

single bullet and of the bullet path, respectively. The obtained ICCD images are post-processed using Matlab by subtracting the average background. A gamma correction factor γ_c is applied to increase the visibility of the plasma [22]. The nozzle and the colors were added in post-processing for illustration purposes. Since the laser and the electric field are both pulsed, it becomes necessary to align them in time, as indicated in figure 3. In order to split the second harmonic (SH) from the input laser beam, a combination of a prism and one dichroic mirror is used. The SH intensity is measured by a photomultiplier tube (Hamamatsu H6779-04) and an infra-red detector (Thorlabs DET36A/M) monitors the laser output intensity. The laser intensity in the focus of the beam is about 10^9 W/cm^2 and 10^{10} W/cm^2 at maximum power for the nanosecond and picosecond laser, respectively. All measurements are conducted in atmospheric pressure air at room temperature.

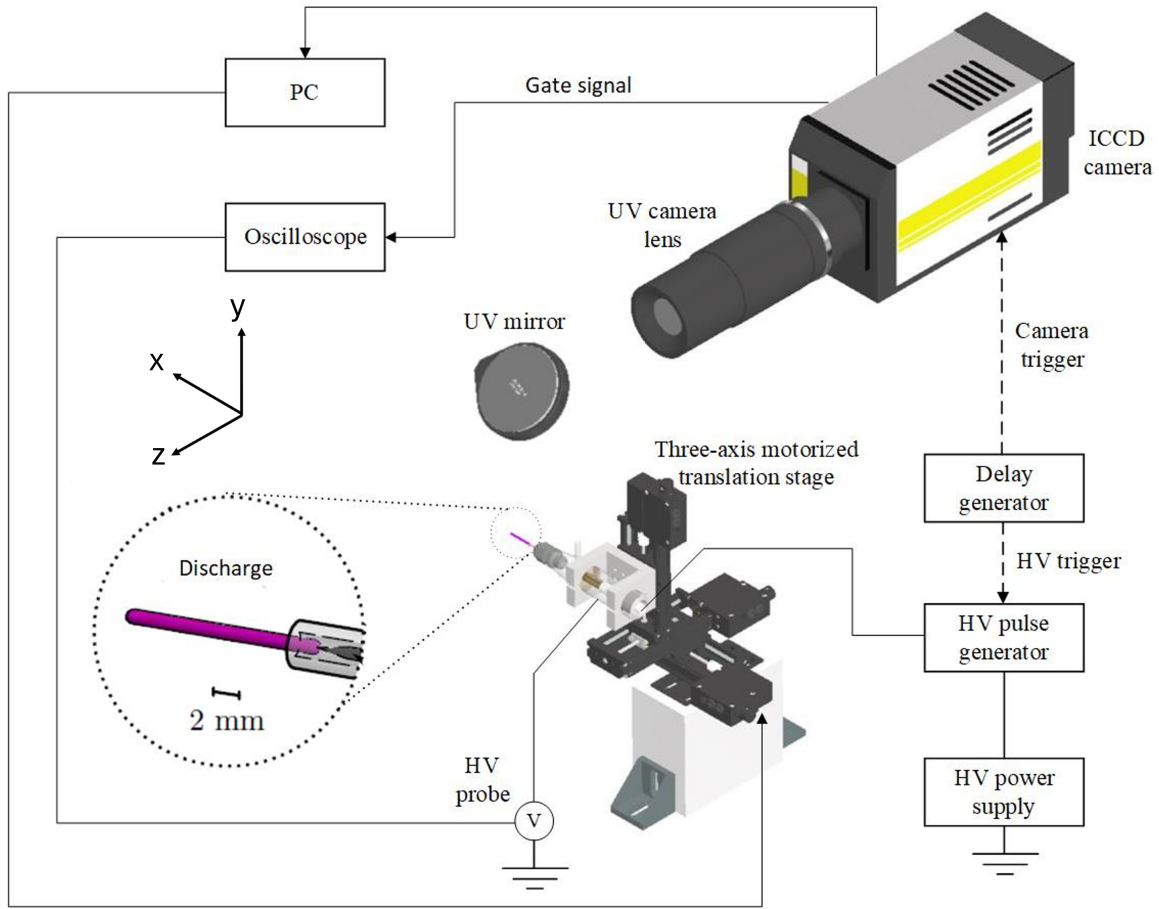


Figure 2: Schematic representation of the set-up used to take the ICCD camera images in Figure 1. The camera is triggered using the delay generator, and it in turn triggers the oscilloscope.

The distance between the needle electrode tip and the laser beam focus is set to 4.0 ± 0.1 mm. Two different E-FISH measurements are performed:

- (i) Radial scan: In order to obtain the radial field distribution, the y -position of the plasma source is changed from -600 till $+600$ μm in steps of 50 μm .
- (ii) Laser intensity scan: This scan is performed to investigate the effect of varying laser input intensity on the E-FISH measurements and the branching. According to [21], the 'effective' intensity of a Gaussian beam is given by

$$I^{\text{GB}} = \mathcal{P}/a_{\text{eff}}, \quad (1)$$

where \mathcal{P} is the laser power and a_{eff} the effective area, defined as

$$a_{\text{eff}} = \frac{\pi w_0^2}{4}, \quad (2)$$

with w_0 the beam waist. Thus, the laser intensity can be varied by either changing the laser power or the beam waist. The input power is varied by changing the

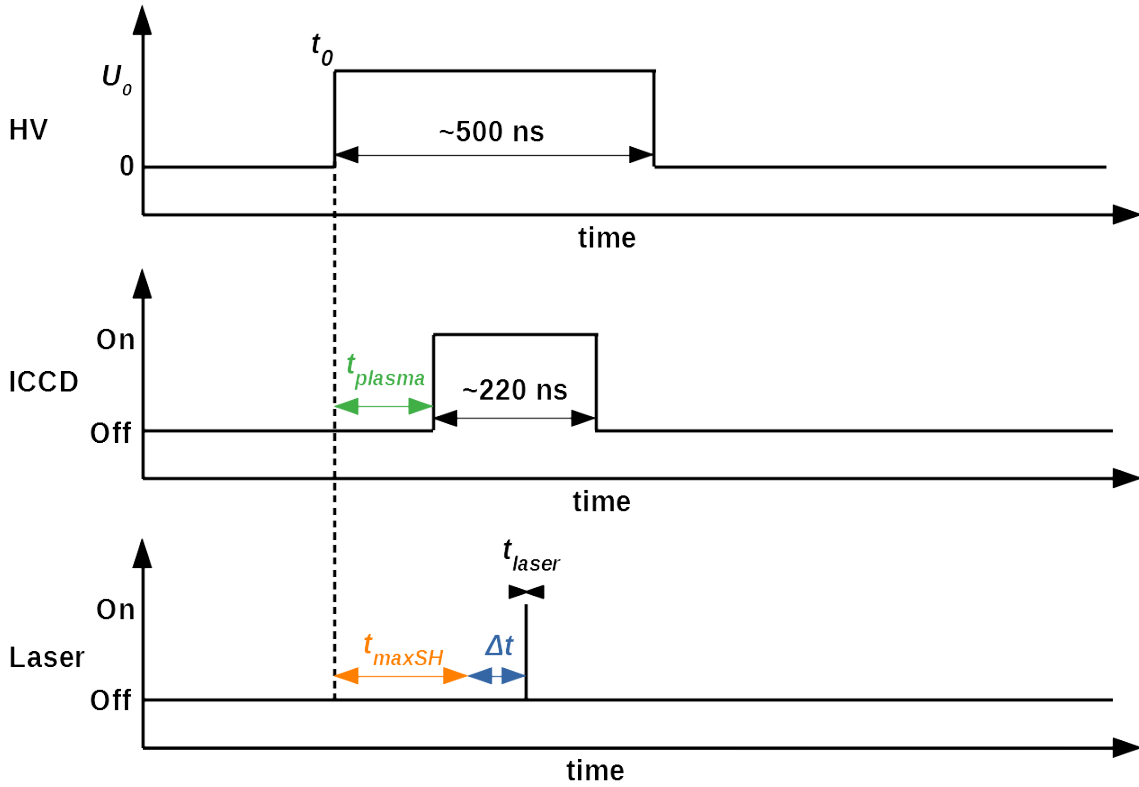


Figure 3: Schematic representation of the HV, laser and camera pulses as they are defined for this set-up. t_0 is defined as the start of the HV pulse. t_{plasma} is the time at which the plasma is first observed. Δt is the variable laser pulse delay, which is centered around the time where the maximum SH intensity is measured t_{maxSH} . Timings are not to scale.

angle orientation of the HWP as is shown in figure 1 in the appendix. Furthermore, several focal length lenses are used to focus the beam, resulting in a different laser intensities around the focus.

3. Results and discussion

3.1. The branching process

In figure 4a, the plasma bullet propagation is shown without a laser beam present. See figure 3 in the appendix for additional images. Inside the main channel, the remnants of previous discharges guide the new streamer, leading to the straight undisturbed plasma bullet trajectory. This is known as the "memory effect" [21, 23, 24].

In figures 4b and 4c, ICCD images obtained with the same settings are shown with the nanosecond and picosecond laser turned on, respectively. See figures 4 and 5 in the appendix for additional images. It can be observed that the path of the jet is changed;

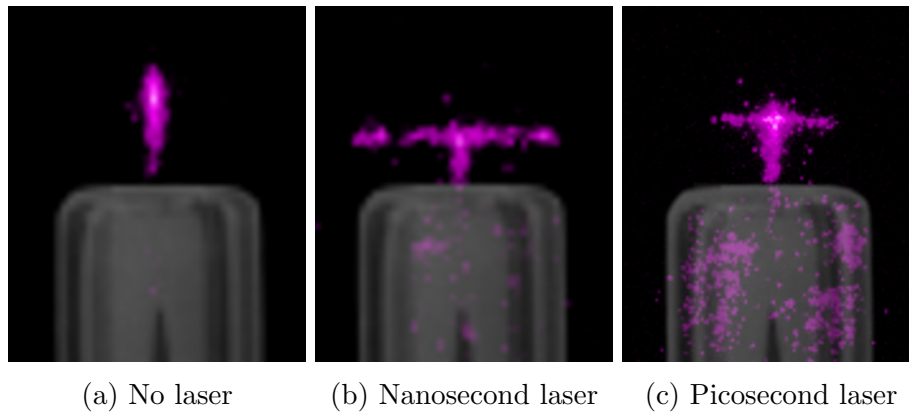


Figure 4: ICCD images for 2 ns gate time of the plasma bullet propagating without the presence of a laser beam (a), with the nanosecond laser (b), and with the picosecond laser (c) turned on. In these images, the laser travels from right to left, while the plasma moves from bottom to top. $\gamma_c = 1.6$ for (a) and (b), and 1.15 for (c).

the plasma is guided into the laser beam path. Furthermore, if branching into the laser path occurs, it always occurs in both directions. Moreover, we identified that the polarization direction of the input light does not matter for the branching. Also, the branching process is very stochastic as can be seen in figure 6 in the appendix.

From figure 5, showing the full trajectory of the branching bullets for the picosecond laser, we can observe that the bullets branch into the laser beam path and at a certain point escape from this path. The bullet follows the electric field lines before and after the branching into the laser beam path. The same holds when using the nanosecond laser as can be seen in figure 2 in the appendix. Moreover, we observed that branches leave the picosecond laser beam closer to the plasma propagation axis compared to using a nanosecond laser. The minimum gate width of the camera is 2 ns, which makes it difficult to assess how long it takes before the branches are created. The branches are at least developed within 2 ns. Given the average speed of the bullets, 10^5 m/s [21], the bullet will move approximately $600 \mu\text{m}$ during a nanosecond laser pulse and $15 \mu\text{m}$ during a picosecond laser pulse. Especially when using the nanosecond laser, the branches are able to develop during the measurement. However, the laser pulse has already past far before the bullet leaves the laser path, which takes about 20 ns for the nanosecond laser and 14 ns for the picosecond laser after branching. Therefore, the difference in guiding is likely due to the electron density induced by the laser diminishing over time, eventually becoming insufficient to confine the bullets, which occurs sooner for the picosecond laser because of the shorter pulse duration.

According to previous research, in gas mixtures with little photo-ionization a streamer discharge tends to travel into the direction of higher electron density [23]. The branching process is shown in figure 6. The electron density in a regular streamer path is around 10^{14}cm^{-3} [25]. We found that the plasma bullet velocity is lower when it branches, which can be explained by the fact that current must be distributed over

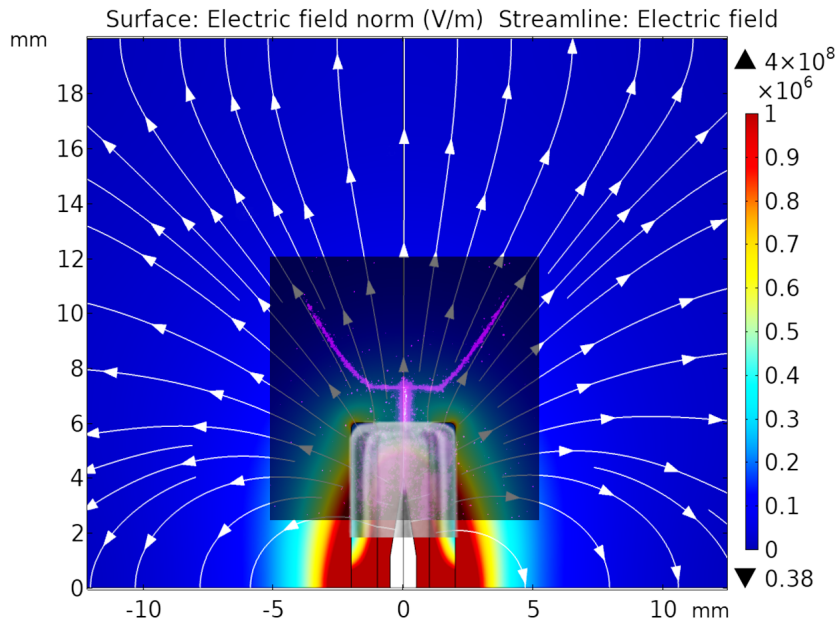


Figure 5: COMSOL Multiphysics model of the electric field streamlines overlaid with an ICCD image with gate time 220 ns of the bullet trajectory for the picosecond laser.

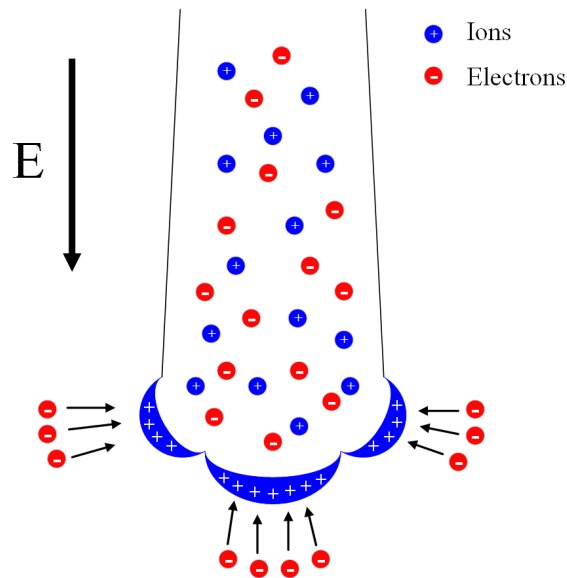


Figure 6: A schematic illustration of a branching event of a streamer discharge, due to the presence of a significant amount of electrons in the laser beam path.

the three paths at the intersection with the laser.

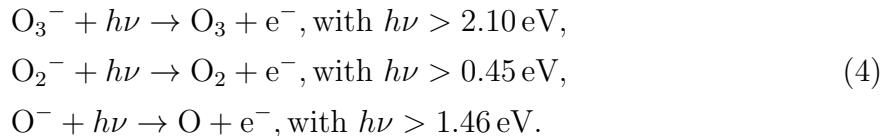
From research on the memory effect, it is determined that electron densities of $10^8 - 10^9 \text{ cm}^{-3}$, which are far below the breakdown threshold, are already sufficient to guide the plasma in a direction nearly perpendicular to the background electric field direction [15]. In order to find the origin of the electrons present in the laser beam path, we need to discuss reactions that generate electrons in our setup.

Positive streamers in air propagate through photoionization of oxygen molecules by ultraviolet (UV) photons emitted by excited nitrogen molecules, because this provides the required free electrons in front of the streamer head. This works as follows: when a high energy electron moving in air collides with a nitrogen molecule and excites it, the nitrogen molecule can subsequently emit a photon with a wavelength of 98 – 102.5 nm. This photon in turn can ionize an oxygen molecule somewhere else, creating an additional electron [26]:



where $h\nu$ represents the photon energy. The process of photoionization stabilizes the discharge front in both the inception cloud phase and in the propagating streamer phase. Besides being created by photoionization, free electrons can also be left over from previous discharges, and can be created by electron detachment from negative ions. Also, external radiation like cosmic rays or bremsstrahlung photons from very fast runaway electrons can act as an electron source [25].

An electron can be released from a negative ion by irradiating the ion with a photon with an energy higher than the detachment energy. The photodetachment of oxygen ions is described as



The photon energy of the used laser (1064 nm) is 1.17 eV. Therefore, only O_2^- is vulnerable to laser induced photodetachment in our setup, because of the higher electron binding energies of O^- and O_3^- (above photon energy) [27]. For the laser power used in this research, O_2^- is almost 100% detached within the laser beam, taking into account the photodetachment cross-section [28]. Thus, photodetachment is the most likely source of the electrons and therefore the branching.

Further away from the center of the studied plasma jet, the mass fraction of nitrogen decreases, as can be observed in figure 7, and subsequently the oxygen concentration increases and more and more photoionization electrons become available, making the streamer less sensitive for variations in background electron density and therefore more difficult to laser guide [15, 25]. This might be the reason for the branches leaving the laser path, because in pure nitrogen, a low concentration of laser-detached electrons is already enough to guide the streamer. This effect is enhanced by the faster attachment of (laser-detached) free electrons at higher oxygen concentrations. Therefore, in high purity nitrogen, there will be more free electrons before the streamer arrives, which can also better guide the streamer. Furthermore, the brightest branching occurs in the region where the mass fraction of N_2 is the highest.

Finally, in theory the laser could also create free electrons in its beam path by direct ionization of gas molecules [15, 16, 29, 30]. The photon energy of the infra-red (IR) input

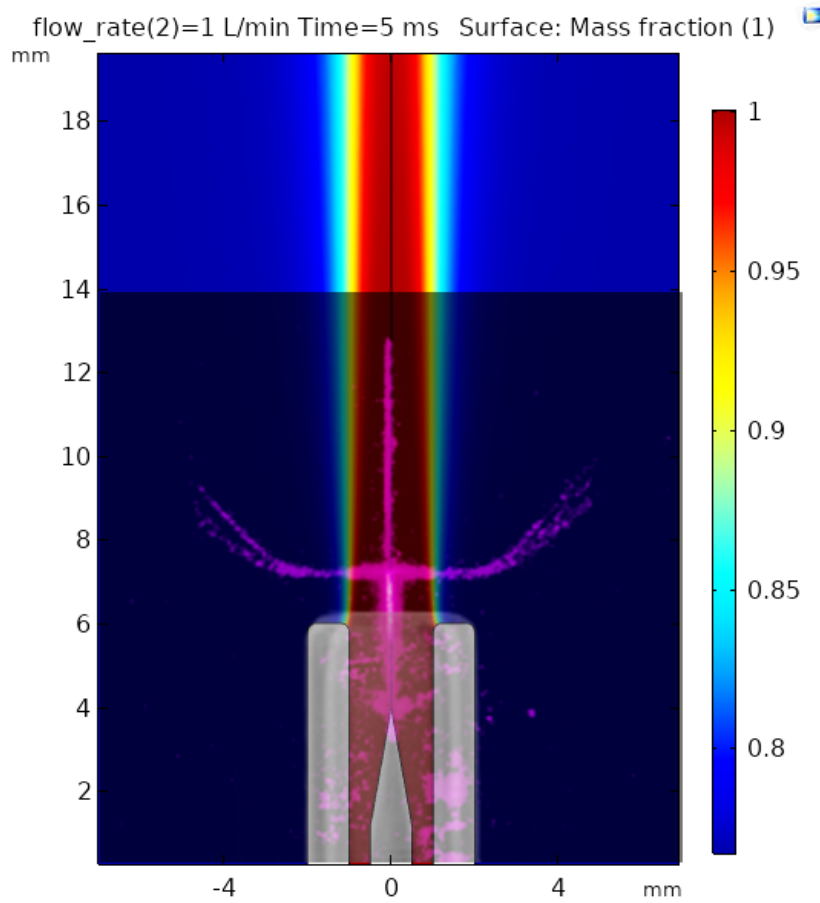


Figure 7: COMSOL Multiphysics model of the mass fraction N_2 for the used plasma nozzle, overlaid with an ICCD image with gate time 170 ns of a branching discharge for the nanosecond laser.

laser is too low to overcome the ionization potential in a single-photon process, but multiple photons together do exceed this barrier and are able to ionize when absorbed simultaneously. For photoionization by the input laser, 11 photons are needed to ionize an oxygen molecule and 14 photons for nitrogen, which are the molecules that are mostly present. The needed laser intensity to cause breakdown due to photoionization using an IR laser is 10^{11} W/cm² [31]. However in this research, the laser intensity in the focus of the beam is over one order of magnitude below this value, especially because we attenuate the beam.

To summarize: the guiding by the laser is most likely a combination of the ions present in the laser beam path due to the previous discharge (memory effect) and the laser detaching the electrons from these negative oxygen ions. The oxygen concentration is high enough to have these negative ions present and the laser intensity is probably too low to ionize oxygen and nitrogen molecules, but high enough to detach electrons from negative oxygen ions.

3.2. Impact of branching on E-FISH measurements

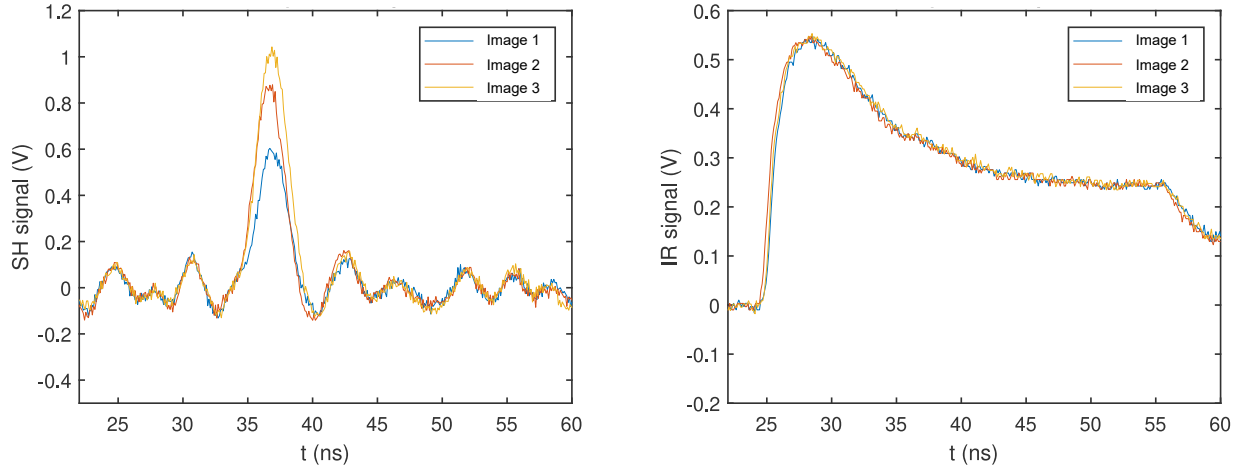
In figure 8, it can be observed that the branching of the jet significantly affects the measured SH signal when using the picosecond laser. When branching occurs, an increase of about 80% in maximum SH signal is measured for a constant IR signal and the same experimental conditions, where the SH signal is shown to decrease for less intense branching. This is the consequence of an increase in electric field length in the laser beam direction when the plasma bullet is traveling into the laser beam, and this field length being far below the coherence length. Similar behavior is observed when using the nanosecond laser. The branches at the end of the jet tend to the left, which is also the position of the post to mount the mirror in the imaging setup in figure 2. This is likely the nearest electrical ground for the plasma.

3.2.1. Radial scan Figure 9c shows that the branching is most apparent around $y = 0 \mu\text{m}$ and decreases with increasing and decreasing y . Additional images can be found in figure 7 in the appendix. The same holds for the ICCD images using the picosecond laser in figure 8 in the appendix. The SH signal measured for the axial and radial field components increases significantly when branching occurs, resulting in a ‘top hat’ profile when using the nanosecond laser, as shown in figure 9a. The profile is expected to gradually decrease for increasing y , but it seems constant for a range of about $500 \mu\text{m}$. Branching was observed in a range of $450 \pm 50 \mu\text{m}$. This exceeds the optical bullet diameter of $280 \pm 20 \mu\text{m}$ [21], but corresponds to the width of the top hat profile. The picosecond E-FISH measurements do not show the top hat profile, but the axial profile is slightly flattened around $y = 0$. The difference is likely caused by a lower laser power, which still provides sufficient E-FISH signal. Additionally, the minimal movement of the bullet during the picosecond laser pulse could also play a role.

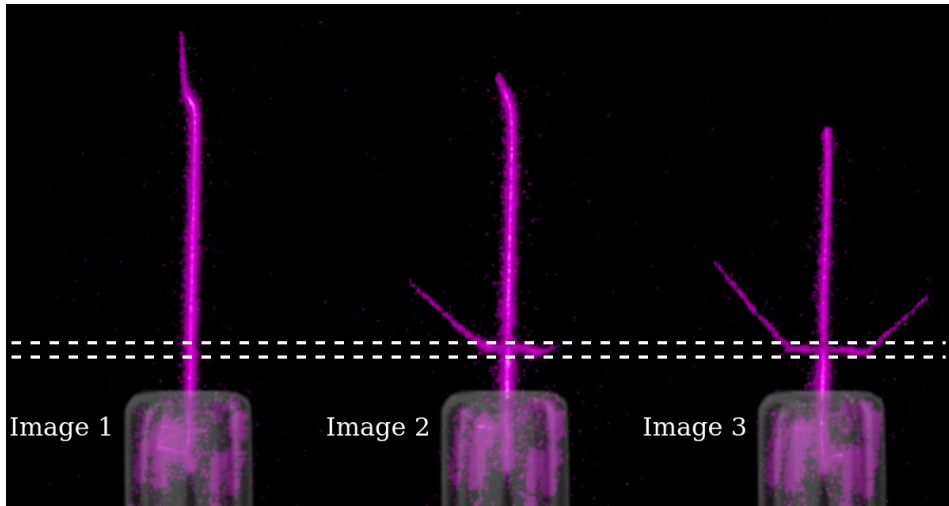
3.2.2. Laser intensity scan The laser power scan, shown in figure 10, reveals a decrease in the measured E-FISH signal for decreasing laser power, in contrast to the constant value expected from theory. The power where the decrease sets in corresponds to the point where the branching starts to decrease in intensity, as can be seen in figure 9 in the appendix. At the input power for which branching no longer occurs, the measurement error is too large to obtain a significant SH signal.

Furthermore, by varying the focal length of the focusing lens, shown in figure 11, it can be observed that the amount of branching of the plasma jet increases for a more focused laser beam.

In order to show the impact of using a lower laser power, the alignment was improved by including more dichroic mirrors as indicated in figure 1, such that a lower input laser power could be used while obtaining similar SH intensities. Subsequently, radial scans are obtained for the different focal length lenses using the nanosecond laser. In figures 12 and 13 the profiles are shown. The top hat profile can again be observed for the 200 mm focal length lens, which is expected from the corresponding branching



(a)



(b)

Figure 8: (a) The SH and IR signal corresponding to the radial electric field component using the picosecond laser, comparing three images with the same experimental parameters. (b) The corresponding ICCD images for 220 ns gate time. In these images, the laser travels from right to left between the two dashed lines, while the plasma moves from bottom to top. $\gamma_e = 1.15$.

behavior in figure 11. Fortunately, the 500 mm focal length lens results look more similar to the expected profiles and the 750 mm results are almost in agreement with literature [21]. There are two main differences: The first difference is the asymmetry in the measured E-FISH signal corresponding to the radial field component that is induced by interference effects, as explained in [32]. The second difference is that the value of the measured E-FISH signal for the radial field component is not zero at $y = 0$, because of the limited spatial resolution when using a lens with a 750 mm focal length.

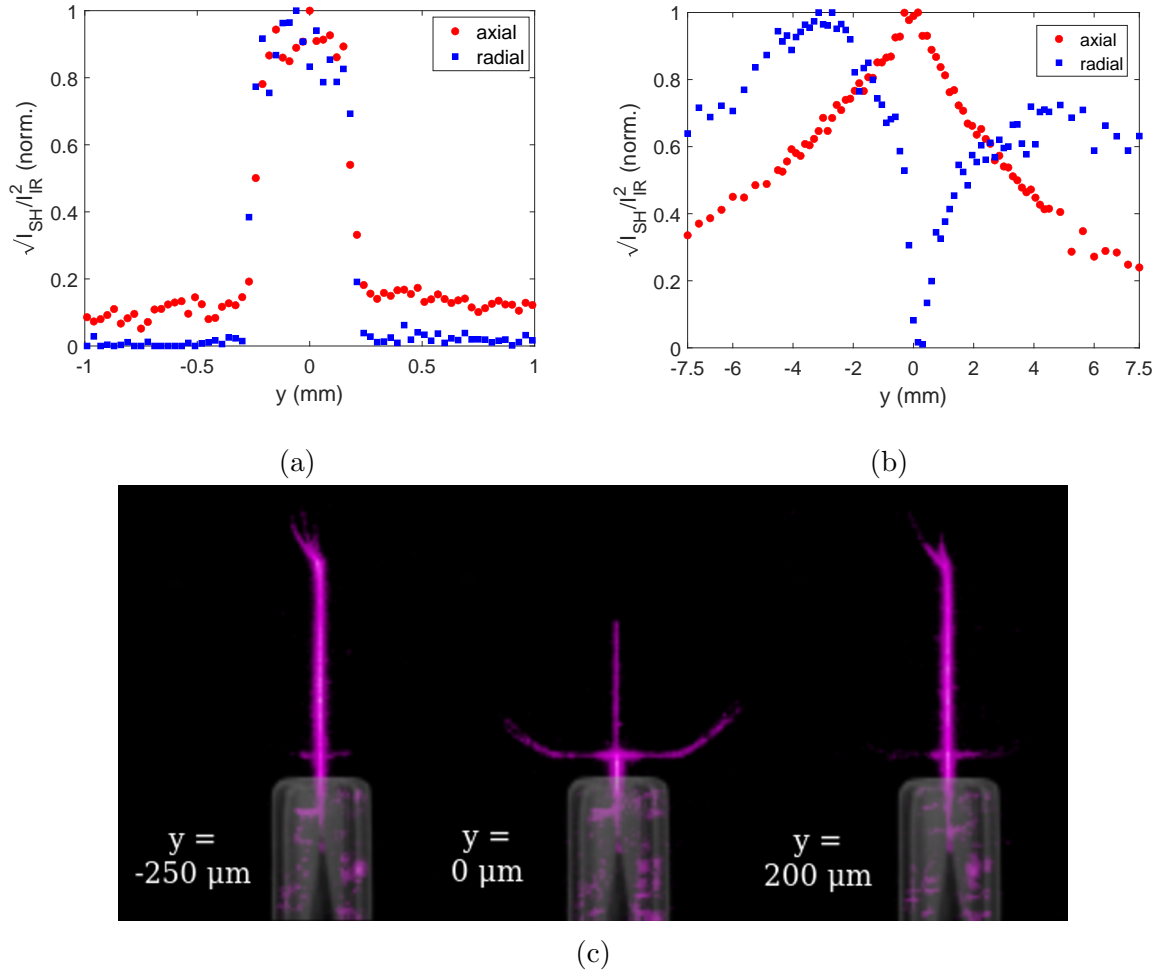


Figure 9: (a) Radial profiles of the E-FISH signal for the axial and radial electric field, obtained with the nanosecond and picosecond laser. The electric field profile corresponding to the nanosecond laser shows an unexpected top hat profile. (b) The corresponding ICCD images for 170 ns gate time for the nanosecond laser. In these images, the laser travels from right to left, while the plasma moves from bottom to top. $\gamma_c = 1.30$.

4. Conclusion

This research reveals an important complication that can occur when performing E-FISH measurements on plasmas that move into the direction of the highest electron density. This issue is also likely present, albeit to a lesser extent, in static plasmas. We found that the probing laser beam, both for picosecond and nanosecond lasers, used during E-FISH measurements has a significant influence on the trajectory of an N_2 ns pulsed plasma jet in atmospheric pressure air. This is due to branching of the plasma into the laser beam path, which is observed by imaging the plasma bullet trajectory. The electrons that induce the branching must be created through photodetachment

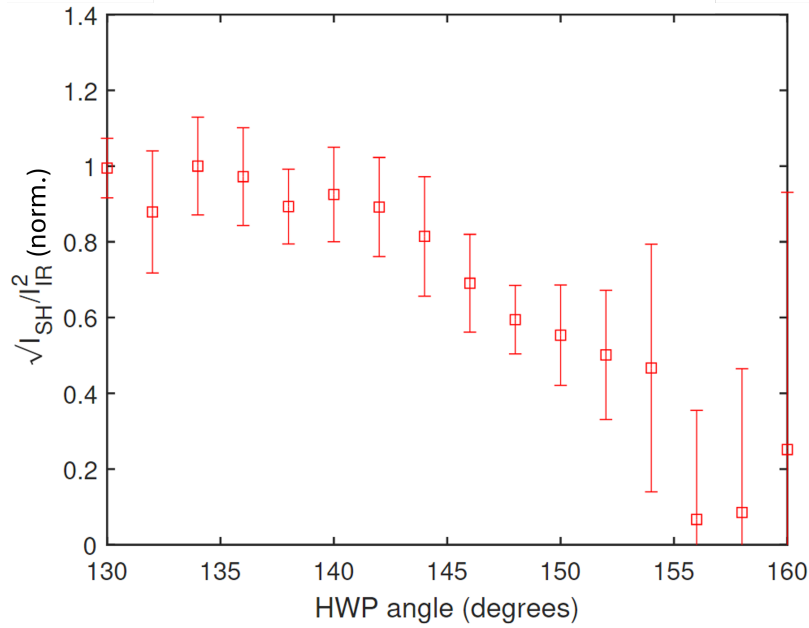


Figure 10: Normalized E-FISH signal for varying HWP angles for the picosecond laser. These angles correspond to varying input laser powers according to figure 1 in the appendix. The axial electric field component is measured.

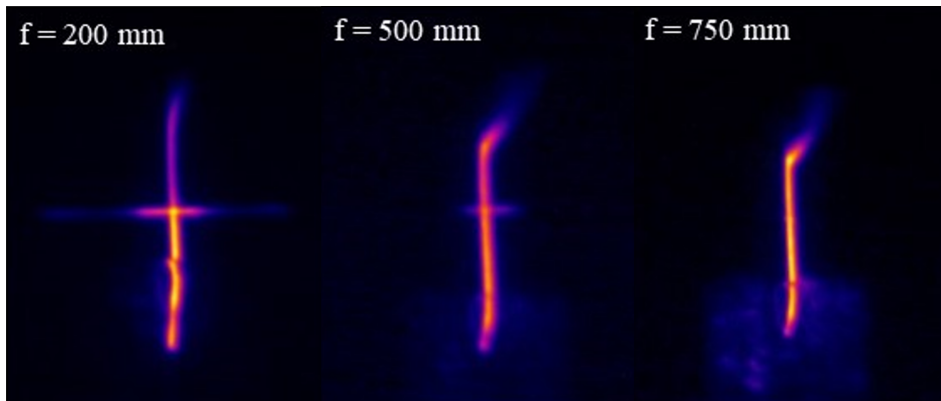
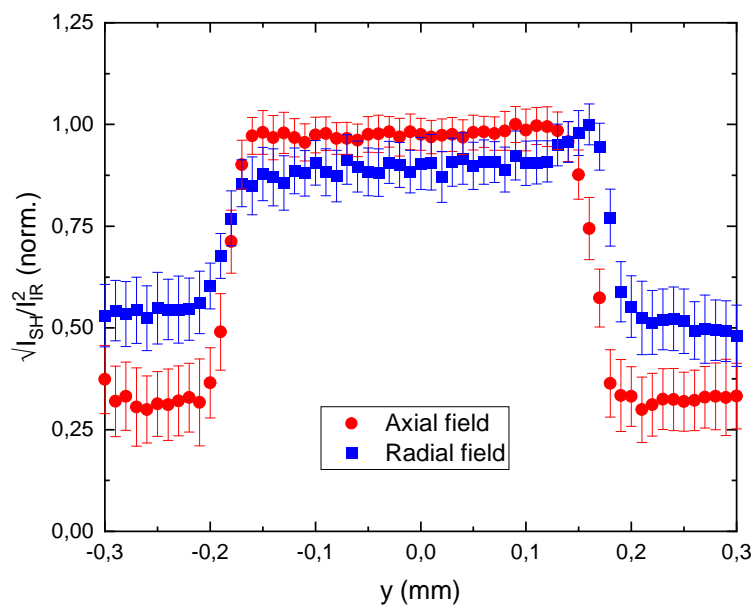
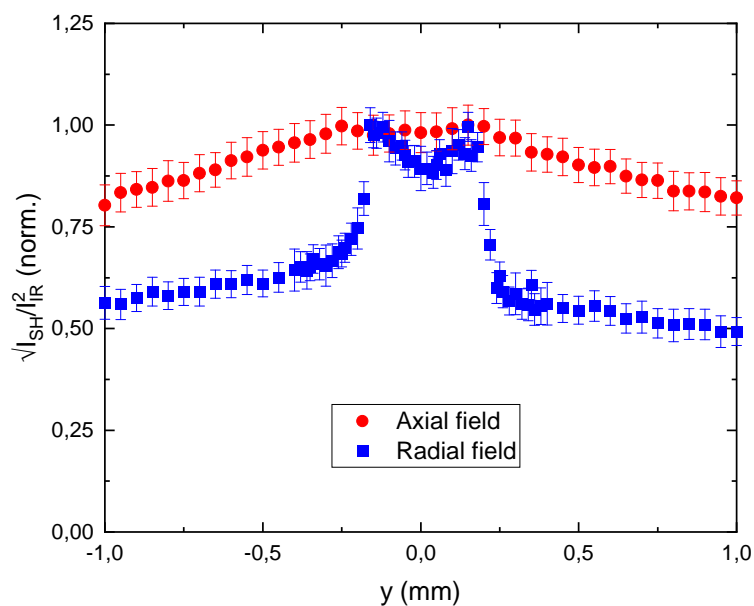


Figure 11: ICCD images (obtained with a Stanford 4 Quick E instead of the Andor iStar camera) of the interaction between the plasma jet and the nanosecond laser for varying focal lengths f of the focusing lens. The gate time of the ICCD was set at 220 ns and all images are an accumulation of 200 frames. The laser travels from right to left, while the plasma moves from bottom to top. Note that the nozzle and the needle electrode are not displayed in these images.



(a) $f = 200$ mm



(b) $f = 500$ mm

Figure 12: Normalized radial profiles of the E-FISH signal corresponding to the axial and radial electric field obtained using the nanosecond laser for varying focal lengths of the focusing lens.

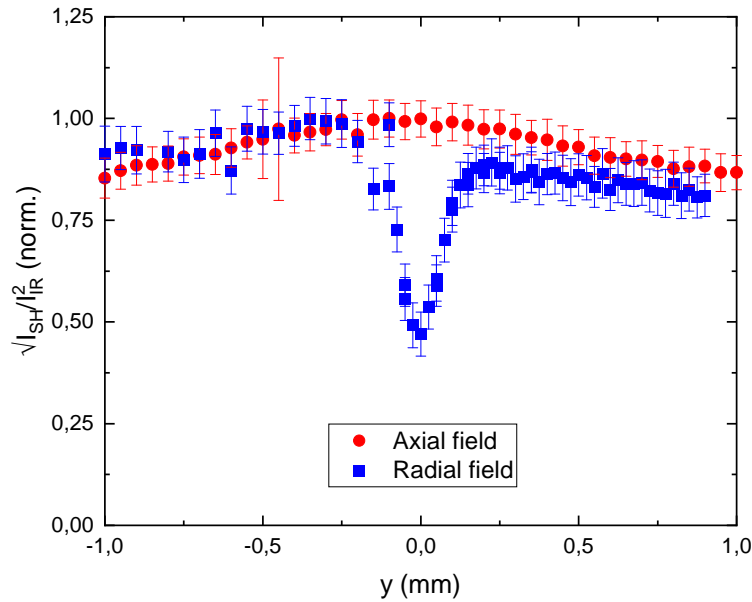
(a) $f = 750$ mm

Figure 13: Continuation of normalized radial profiles of the E-FISH signal corresponding to the axial and radial electric field obtained using the nanosecond laser for varying focal lengths of the focusing lens.

reactions as the laser power is deemed too low for laser induced breakdown. After leaving the laser path, which is due to electrons shielding the streamer head as a result of a higher oxygen concentration, the streamer branches again follow the field lines of the background electric field.

The effect of pulse duration of the probing laser beam is investigated by comparing the branching behavior and the E-FISH signal obtained with a picosecond and a nanosecond laser. We determined that the branch formation takes place on a timescale below 2 ns. Therefore, the formation occurs completely during a nanosecond laser pulse. It is shown that branches result in a higher SH intensity. For nanosecond E-FISH measurements, when the SH signal is measured at different radial positions in the plasma, the obtained profile is completely determined by the branching behavior. For a 150 ps pulsed laser beam, it is found that the E-FISH measurements are not affected by the branching.

Non-invasive E-FISH measurements can be achieved by using (either) a lower laser power at the plasma-laser intersection and/or a shorter pulse duration. The decrease in branching intensity for a less focused laser beam (and thus lower laser power), results in an increasing accuracy of the electric profile, nonetheless, at the expense of spatial resolution. Similarly, decreasing the laser input power results in more accurate measurements with loss of signal-to-noise. However, recent work has shown that low laser power E-FISH measurements are possible [33].

Appendix

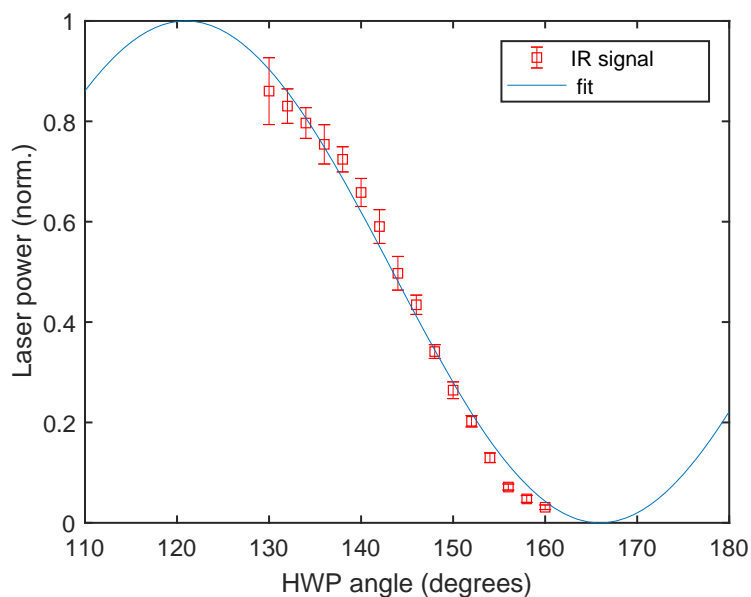


Figure 1: Measured IR signal (red) for varying angles of the half-wave plate for the picosecond laser, with a fit (blue) based on Malus' Law [34] adjusted for the HWP properties. Both the data and the fit have been normalized using the maximum of the fit.

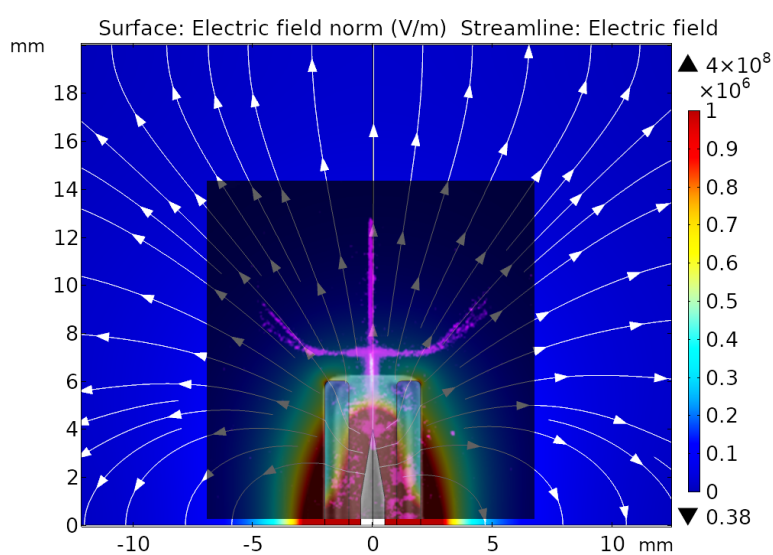


Figure 2: COMSOL Multiphysics model of the electric field streamlines compared to an ICCD image with gate time 220 ns of the bullet trajectory for the picosecond laser.

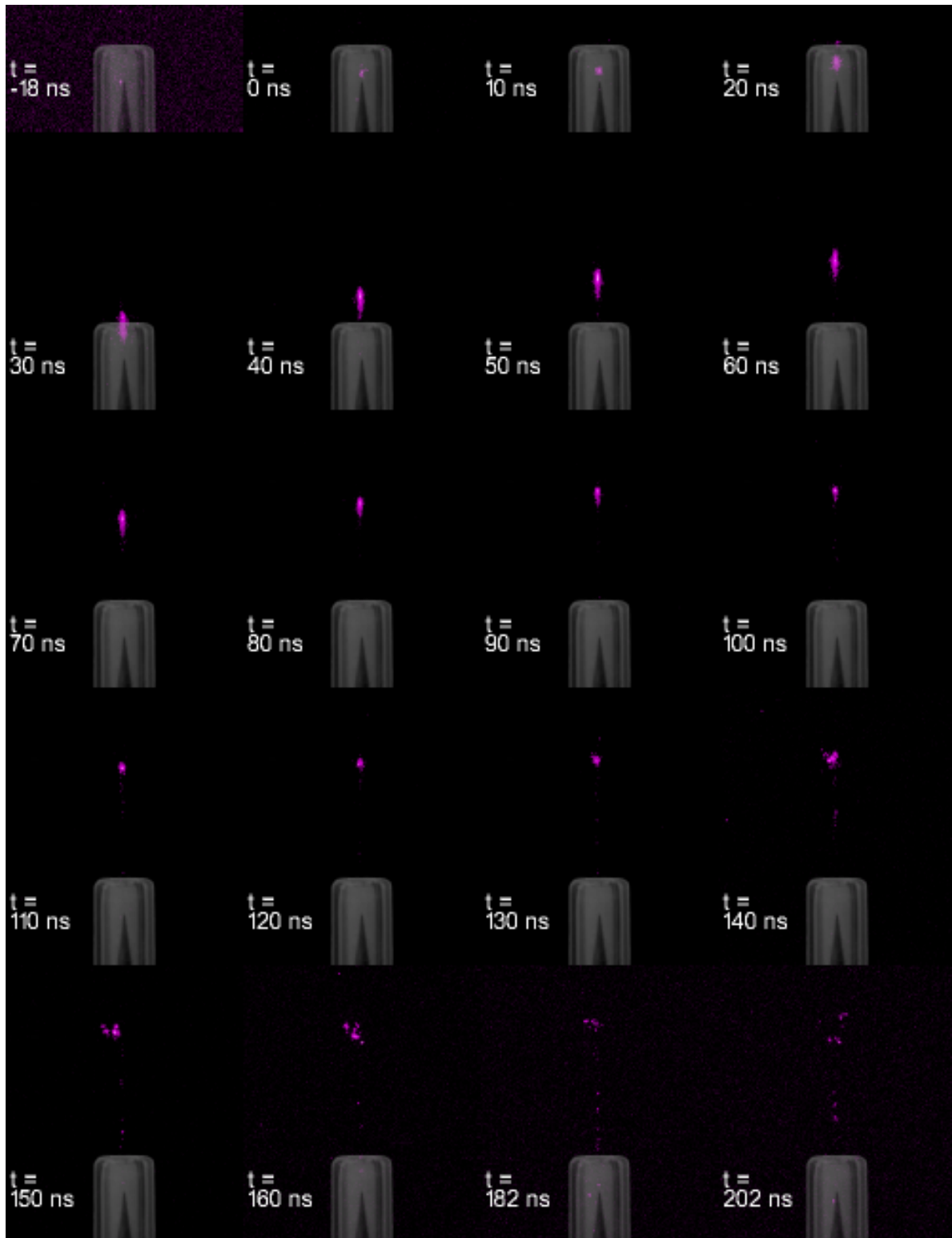


Figure 3: The plasma bullet trajectory with laser off, an exposure time of 2 ns. At $t = -18$ ns, the HV pulse is sent to the plasma source. $\gamma_c = 1.6$.

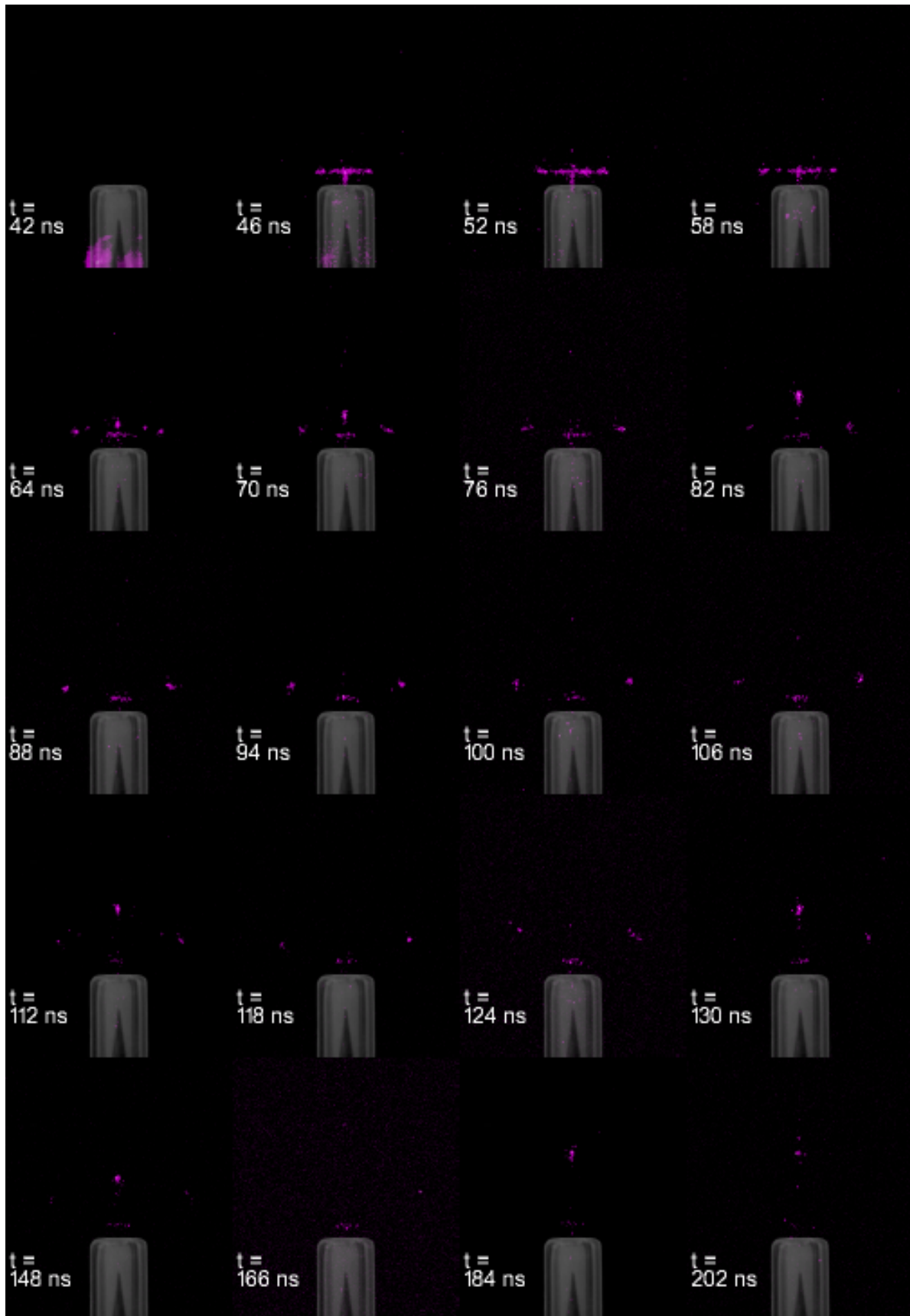


Figure 4: The plasma bullet with the nanosecond laser turned on. The exposure time is 2 ns. $\gamma_c = 1.6$.

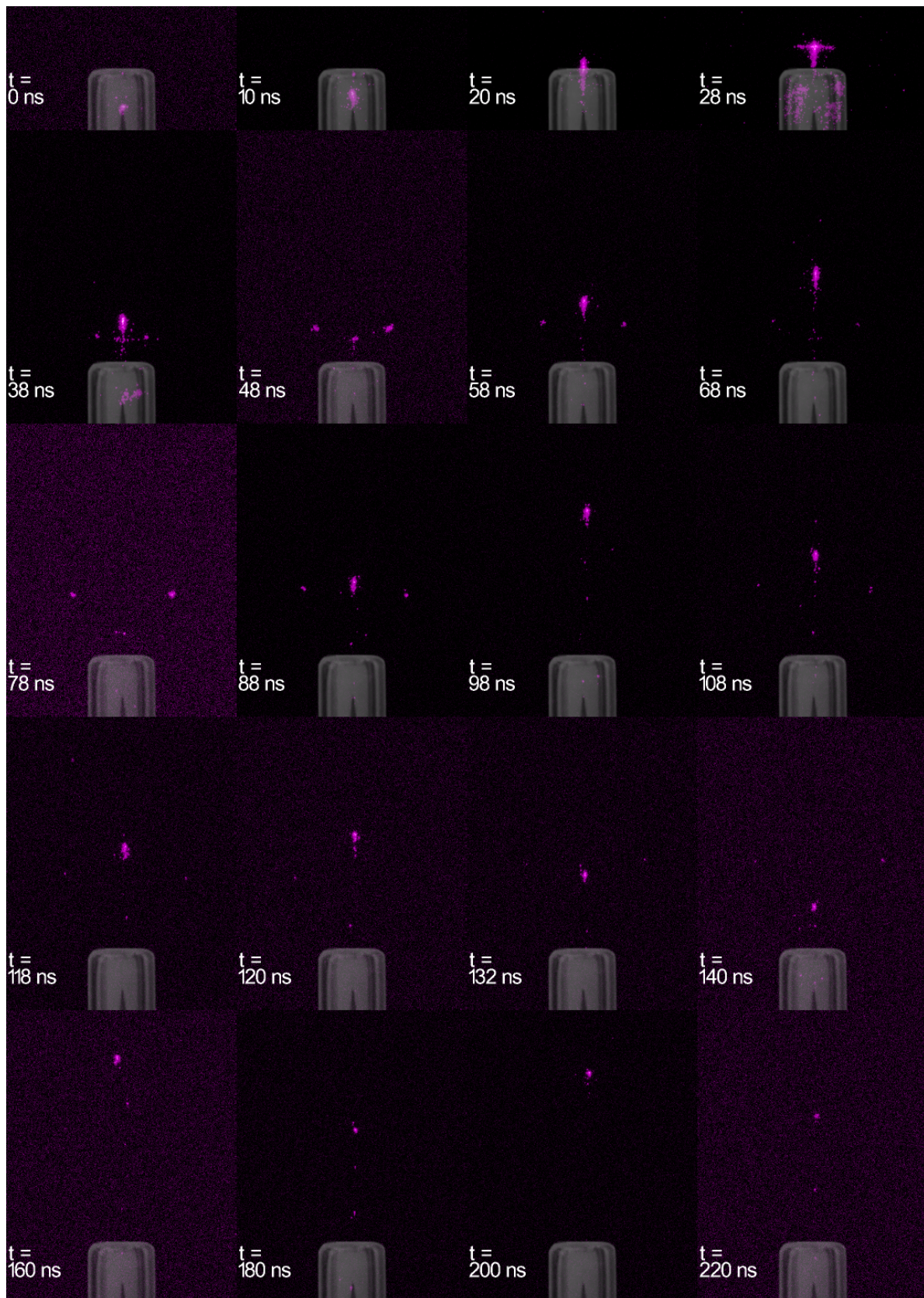


Figure 5: The plasma bullet with the picosecond laser turned on. The exposure time is 2 ns. $\gamma_c = 1.15$.

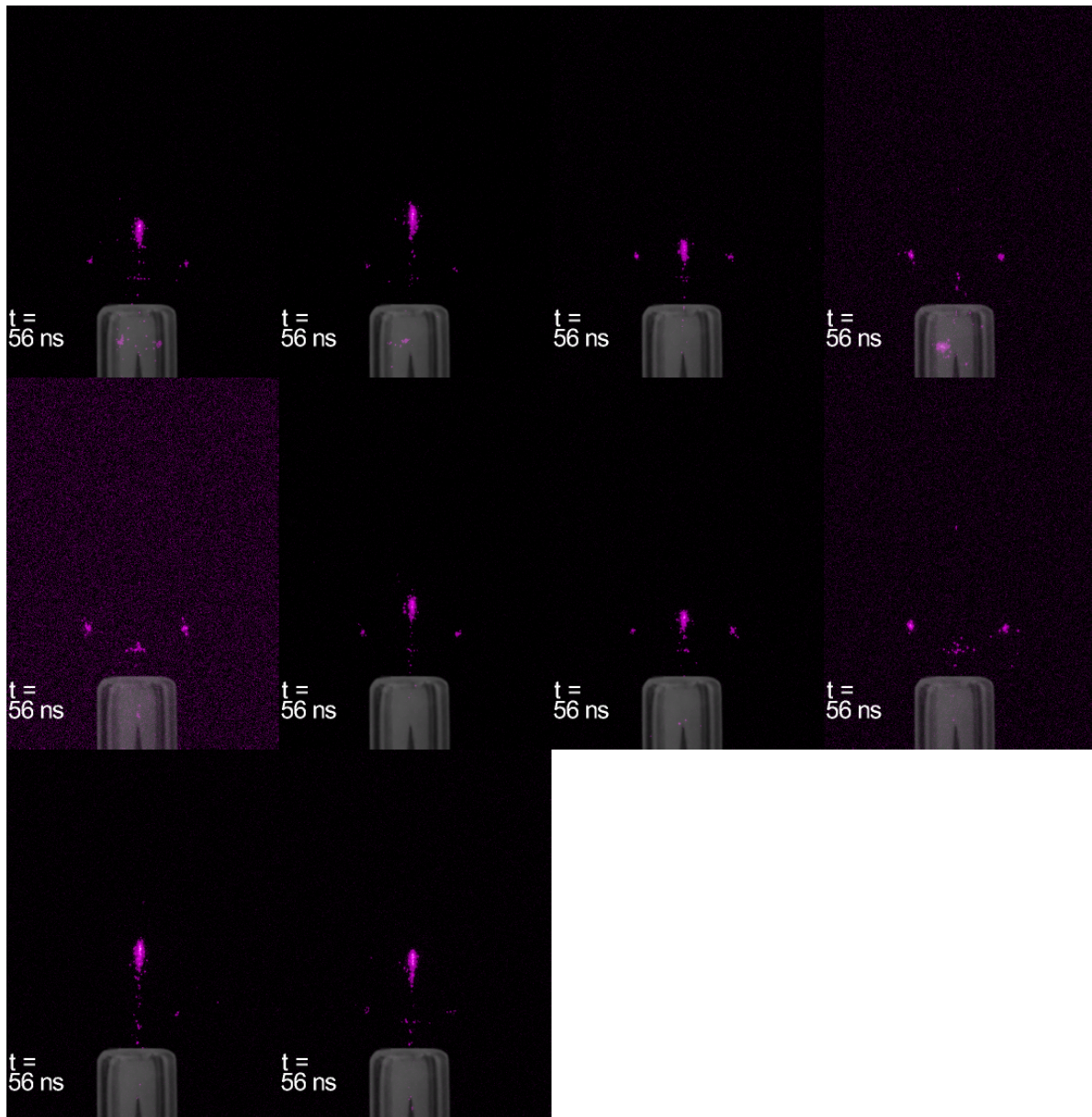


Figure 6: The plasma bullet at $t = 56$ ns with the picosecond laser turned on. The exposure time is 2 ns. The experimental parameters do not vary, but the occurrence and intensity of the branches clearly vary between bullets. $\gamma_c = 1.15$.

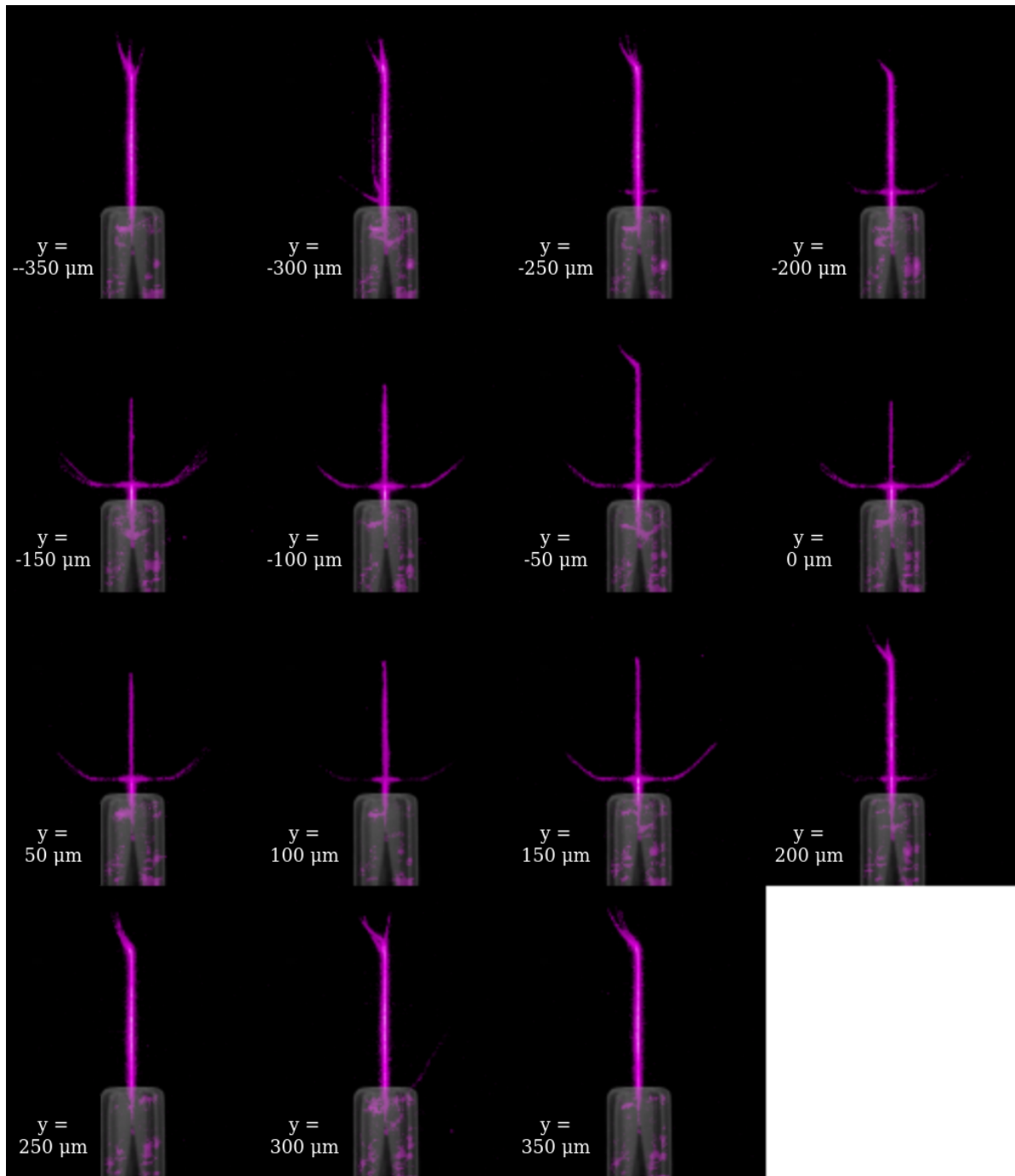


Figure 7: The plasma jet for varying radial positions using 170 ns exposure time with the nanosecond laser turned on. $\gamma_c = 1.30$.

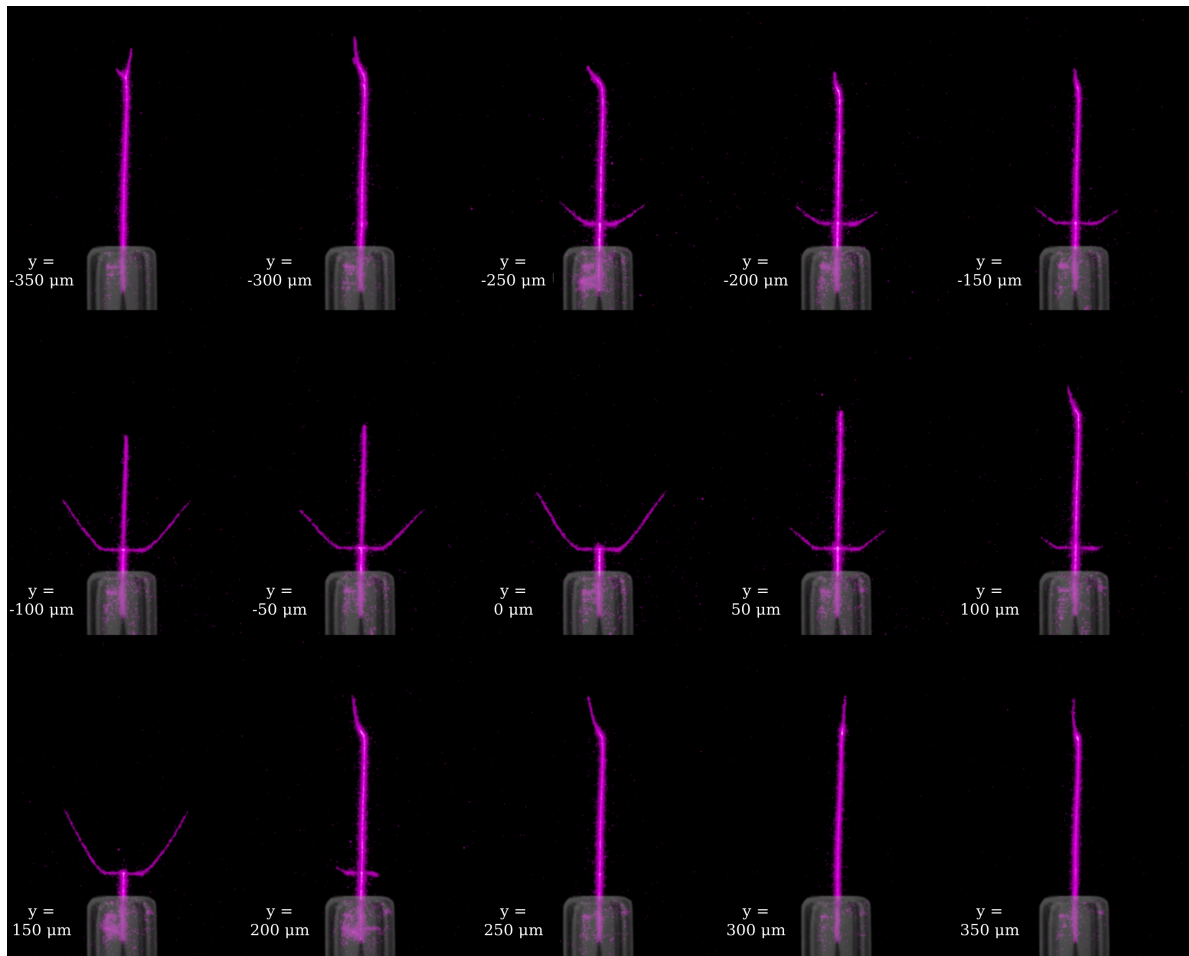


Figure 8: The plasma jet for varying radial positions using 220 ns exposure time with the picosecond laser turned on. $\gamma_c = 1.15$.

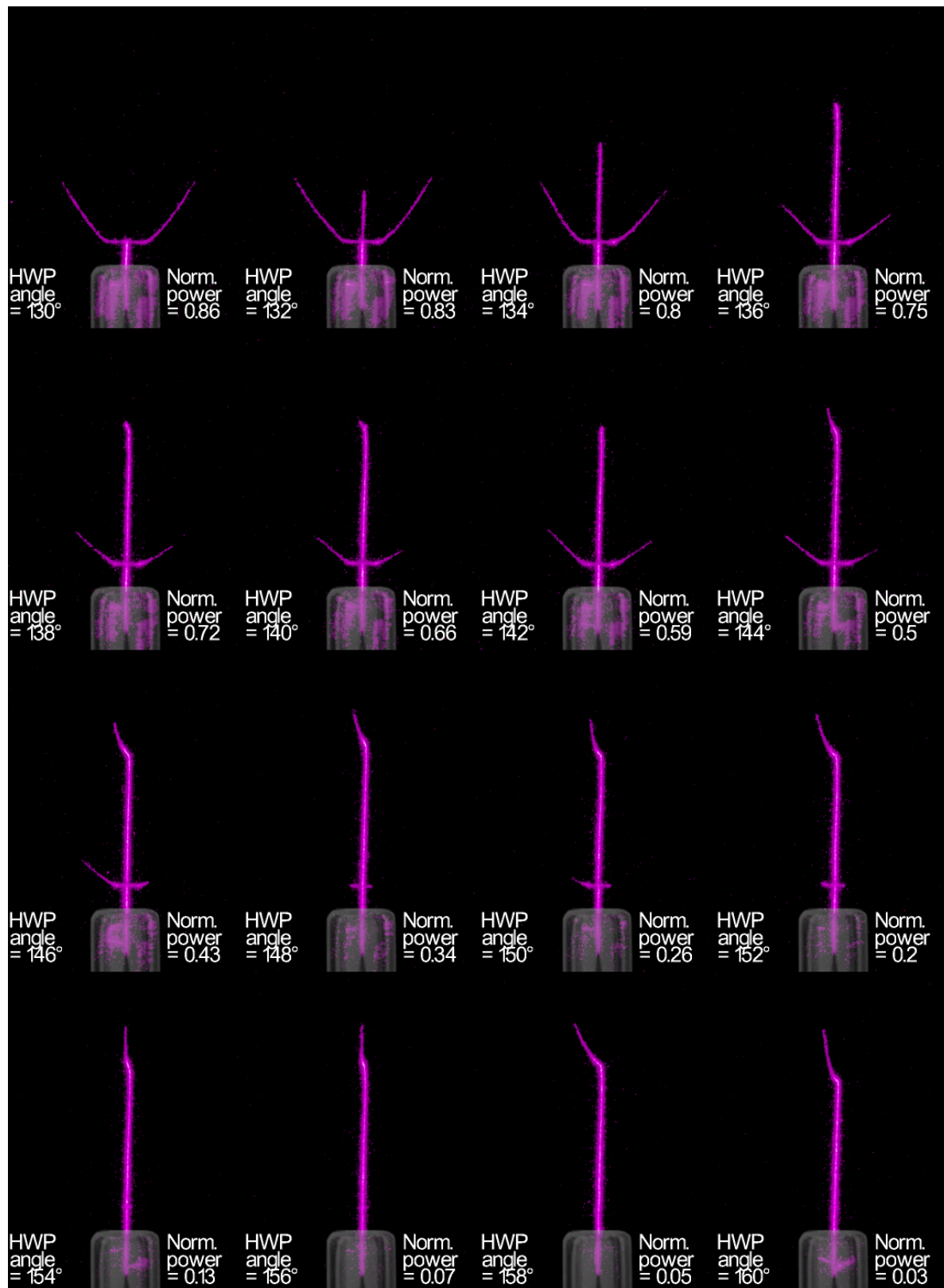


Figure 9: The plasma jet for varying input laser powers of the picosecond laser, using 220 ns exposure time. The normalized powers of the input laser for each HWP angle are given based on Figure 1. $\gamma_c = 1.15$.

References

- [1] Simon Hübner, Joao Santos Sousa, Joost van der Mullen, and William G Graham. Thomson scattering on non-thermal atmospheric pressure plasma jets. *Plasma Sources Science and Technology*, 24(5):054005, aug 2015.
- [2] A.K. Patnaik, I. Adamovich, J.R. Gord, and S. Roy. Recent advances in ultrafast-laser-based spectroscopy and imaging for reacting plasmas and flames. *Plasma Sources Science and Technology*, 26(10):103001, sep 2017.
- [3] K.V. Kozlov and H.-E. Wagner. Progress in spectroscopic diagnostics of barrier discharges. *Contributions to Plasma Physics*, 47(1-2):26–33, feb 2007.
- [4] A Sobota, O Guaitella, G B Sretenović, I B Krstić, V V Kovačević, A Obrusník, Y N Nguyen, L Zajíčková, B M Obradović, and M M Kuraica. Electric field measurements in a kHz-driven He jet—the influence of the gas flow speed. *Plasma Sources Science and Technology*, 25(6):065026, nov 2016.
- [5] K V Kozlov, H-E Wagner, R Brandenburg, and P Michel. Spatio-temporally resolved spectroscopic diagnostics of the barrier discharge in air at atmospheric pressure. *Journal of Physics D: Applied Physics*, 34(21):3164, oct 2001.
- [6] R Tschiersch, M Bogaczyk, and H.E. Wagner. Systematic investigation of the barrier discharge operation in helium, nitrogen, and mixtures: discharge development, formation and decay of surface charges. *Journal of Physics D: Applied Physics*, 47(36):365204, aug 2014.
- [7] E.T. Slikboer. *Investigation of plasma surface interactions using Mueller Polarimetry*. PhD thesis, Eindhoven University of Technology, 2018. Available at <https://research.tue.nl/en/publications/investigation-of-plasma-surface-interactions-using-mueller-polari>.
- [8] Elmar Slikboer, Olivier Guaitella, and Ana Sobota. Time-resolved electric field measurements during and after the initialization of a kHz plasma jet—from streamers to guided streamers. *Plasma Sources Science and Technology*, 25(3):03LT04, may 2016.
- [9] A. Dogariu, B.M. Goldberg, S. O’Byrne, and R.B. Miles. Species-independent femtosecond localized electric field measurement. *Physical Review Applied*, 7(024024), February 2017.
- [10] T.L. Chng, M. Naphade, B.M. Goldberg, I.V. Adamovich, and S.M. Starikovskaia. Electric field vector measurements via nanosecond electric-field-induced second-harmonic generation. *Optical Letters*, 45, 2020.
- [11] X. Lu and M. Laroussi. Dynamics of an atmospheric pressure plasma plume generated by submicrosecond voltage pulses. *Journal of Applied Physics*, 100, 2006.
- [12] S. Hofmann, A. Sobota, and P. Bruggeman. Transitions between and control of guided and branching streamers in DC nanosecond pulsed excited plasma jets. *IEEE Transactions on Plasma Science*, 40(11):2888–2899, nov 2012.
- [13] XinPei Lu and Kostya (Ken) Ostrikov. Guided ionization waves: The physics of repeatability. *Applied Physics Reviews*, 5(3):031102, 07 2018.
- [14] B.M. Goldberg, T. Hoder, and R. Brandenburg. Electric field determination in transient plasmas: in situ & non-invasive methods. *Plasma Sources Science and Technology*, 31(7):073001, sep 2022.
- [15] S. Nijdam, J. Teunissen, E. Takahashi, and U. Ebert. The role of free electrons in the guiding of positive streamers. *Plasma Sources Science and Technology*, 25(4), May 2016.
- [16] S. Nijdam, E. Takahashi, J. Teunissen, and U. Ebert. Streamer discharges can move perpendicularly to the electric field. *New Journal of Physics*, 16(103038), October 2014.
- [17] Shin Nakamura, Masataka Sogame, Masahiro Sato, Takashi Fujii, and Akiko Kumada. Electric field measurement in dc corona discharge in atmospheric pressure air using E-FISHG and laser-triggering methods. *Plasma Sources Science and Technology*, 33, 05 2024.
- [18] C. DeMichelis. Laser induced gas breakdown: A bibliographical review. *IEEE Journal of Quantum Electronics*, 5(4):188–202, apr 1969.
- [19] Igor V Adamovich, Tom Butterworth, Thomas Orriere, David Z Pai, Deanna A Lacoste, and

- Min Suk Cha. Nanosecond second harmonic generation for electric field measurements with temporal resolution shorter than laser pulse duration. *Journal of Physics D: Applied Physics*, 53(14):145201, jan 2020.
- [20] B.M. Goldberg, T.L. Chng, A. Dogariu, and R.B. Miles. Electric field measurements in a near atmospheric pressure nanosecond pulse discharge with picosecond electric field induced second harmonic generation. *Applied Physics Letters*, 112(064102), February 2018.
- [21] M. van der Schans. *Experiments on the physics of pulsed plasma jets*. PhD thesis, Eindhoven University of Technology, December 2018. Available at <https://research.tue.nl/en/publications/experiments-on-the-physics-of-pulsed-plasma-jets>.
- [22] David R. Bull. Chapter 4 - digital picture formats and representations. In David R. Bull, editor, *Communicating Pictures*, pages 99–132. Academic Press, Oxford, 2014.
- [23] S Nijdam, E Takahashi, A H Markosyan, and U Ebert. Investigation of positive streamers by double-pulse experiments, effects of repetition rate and gas mixture. *Plasma Sources Science and Technology*, 23(2):025008, mar 2014.
- [24] Y Li, E M van Veldhuizen, G J Zhang, U Ebert, and S Nijdam. Positive double-pulse streamers: how pulse-to-pulse delay influences initiation and propagation of subsequent discharges. *Plasma Sources Science and Technology*, 27(12):125003, dec 2018.
- [25] Sander Nijdam, Jannis Teunissen, and Ute Ebert. The physics of streamer discharge phenomena. *Plasma Sources Science and Technology*, 29(10):103001, nov 2020.
- [26] G Wormeester, S Pancheshnyi, A Luque, S Nijdam, and U Ebert. Probing photo-ionization: simulations of positive streamers in varying N₂O₂-mixtures. *Journal of Physics D: Applied Physics*, 43(50):505201, dec 2010.
- [27] M Hasani, Z Marvi, and J Beckers. Probing negative ions and electrons in the afterglow of a low-pressure oxygen radiofrequency plasma using laser-induced photodetachment. *Journal of Physics D: Applied Physics*, 54(49):495202, sep 2021.
- [28] D. S. Burch, S. J. Smith, and L. M. Branscomb. Photodetachment of O₂⁻. *Phys. Rev.*, 112:171–175, Oct 1958.
- [29] S. B. Leonov, A. A. Firsov, M. A. Shurupov, J. B. Michael, M. N. Shneider, R. B. Miles, and N. A. Popov. Femtosecond laser guiding of a high-voltage discharge and the restoration of dielectric strength in air and nitrogen. *Physics of Plasmas*, 19(12):123502, 12 2012.
- [30] V D Zvorykin, A O Levchenko, and N N Ustinovskii. Control of extended high-voltage electric discharges in atmospheric air by UV KrF-laser radiation. *Quantum Electronics*, 41(3):227, mar 2011.
- [31] Zhixing Gao, Lixuan Han, and Jing Li. Investigation of laser induced air breakdown thresholds at 1064, 532, 355, 266 and 248nm. In *Pacific Rim Laser Damage 2019: Optical Materials for High-Power Lasers*, 2019.
- [32] Yihao Guo, Anne Limburg, Jesse Laarman, Jannis Teunissen, and Sander Nijdam. Measurement of the electric field distribution in streamer discharges, 2024.
- [33] J Kuhfeld, N D Lepikhin, D Luggenhölscher, and U Czarnetzki. Vibrational cars measurements in a near-atmospheric pressure plasma jet in nitrogen: I. measurement procedure and results. *Journal of Physics D: Applied Physics*, 54(30):305204, may 2021.
- [34] C.A. Bennet. *Principles of Physical Optics*. John Wiley & Sons, Inc., illustrated edition, 2008.